Optics Letters

Highly tunable birefringent phase-matched second-harmonic generation in an angle-cut lithium niobate-on-insulator ridge waveguide

Chuanyi Lu,[1] Yuting Zhang,[1] Jing Qiu,[2] Yongzhi Tang,[1] Tingting Ding,[3] Shijie Liu,[1] Yuanlin Zheng,[1,4,6] and Xianfeng Chen[1,2,3,5,7]

[1]State Key Laboratory of Advanced Optical Communication Systems and Networks, School of Physics and Astronomy, Shanghai Jiao Tong University, Shanghai 200240, China
[2]Jinan Institute of Quantum Technology, Jinan 250101, China
[3]School of Electronic and Electrical Engineering, Shanghai University of Engineering Science, Shanghai 201620, China
[4]Shanghai Research Center for Quantum Sciences, Shanghai 201315, China
[5]Collaborative Innovation Center of Light Manipulations and Applications, Shandong Normal University, Jinan 250358, China
[6]e-mail: ylzheng@sjtu.edu.cn
[7]e-mail: xfchen@sjtu.edu.cn

Received 24 November 2021; revised 10 January 2022; accepted 17 January 2022; posted 18 January 2022; published 18 February 2022

Phase-matched nonlinear wave mixing, e.g., second-harmonic generation (SHG), is crucial for frequency conversion for integrated photonics and applications, where phase matching wavelength tunability in a wide manner is important. Here, we propose and demonstrate a novel design of angle-cut ridge waveguides for SHG on the lithium niobate-on-insulator (LNOI) platform via type-I birefringent phase matching (BPM). The unique strong birefringence of LN is used to achieve flexible temperature tuning. We experimentally demonstrate a normalized BPM conversion efficiency of 2.7%$W^{-1}cm^{-2}$ in an angle-cut LN ridge waveguide with a thermo tuning slope of 1.06 nm/K at the telecommunication C band. The approach effectively overcomes the spatial walk-off effect and avoids the need for periodic domain engineering. Furthermore, the angle-cut ridge waveguide scheme can be universally extended to other on-chip birefringent platforms where domain engineering is difficult or immature. The approach may open up an avenue for tunable nonlinear frequency conversion on integrated photonics for broad applications.

https://doi.org/10.1364/OL.449634

Quadratic nonlinear processes are widely applied for many vital applications ranging from optical frequency conversion [1–4], tunable coherent radiation [5,6] to quantum information processing [7–9]. Lithium niobate (LN), a multifunctional ferroelectric crystal with excellent properties including low absorption loss, wide transparency window, large electro-optic coefficient, and strong second-order nonlinearity, has been playing an important role in these areas. It is often referred to as the "silicon of photonics". Especially, the recent revolution of the lithium niobate-on-insulator (LNOI) technology has attracted considerable attention [10–14]. The characteristics of high index contrast between the on-top LN and underneath silica layer, combined with micro/nano-scale photonic structures, makes it possible to achieve high-density photonic integration on LNOI. Additionally, the tight confinement of optical fields could dramatically enhance light–matter interaction and boost performance for superior integrated components. Therefore, the LNOI platform has a great potential for realizing multi-functional, high-performance photonic devices and opens up new possibilities for next-generation integrated (nonlinear) photonics [15–21].

To date, remarkable advances have been made in quadratic optical parametric processes on the LNOI platform, which are crucial in both classical and quantum optics. Among them, second-harmonic generation (SHG) is one of the most prominent applications. For efficient SHG, it is necessary to satisfy energy and momentum conservations simultaneously. However, due to the material and waveguide structure dispersion, the momentum during wave mixing is naturally not conserved, i.e., phase mismatching. There are several phase-matching mechanisms, which can be roughly divided into quasi-phase matching (QPM), intermodal phase matching (intermodal PM), and birefringent phase matching (BPM). QPM is a popular approach which uses the reciprocal lattice vector provided by periodic domain inversion to compensate for the phase mismatch [1,2,5,19–26]. The method can take advantage of the largest nonlinear coefficient and has a wide operation wavelength range upon QPM grating design. However, the periodic poling is material selective and only applicable to ferroelectric crystals. In addition, due to stronger dispersion, nonlinear wave mixings in LNOI waveguides requires smaller poling periods than their bulk counterparts. Also, period poling requires stringent domain uniformity where any discrepancy would decrease the actual conversion efficiency. These all impose difficulties to the poling technique. Furthermore, the type-0 phase-matching scheme, usually adopted for QPM to use the largest nonlinear coefficient, suffers from a limited wavelength tunability due to the relatively weak wavelength dependence on the thermo-optic coefficient. Another common method is intermodal PM, which

is typically achieved by engineering the waveguide mode dispersion between the fundamental mode of pump and higher-order second harmonic (SH) modes. Such highly tunable efficient SHG via type-I intermodal PM has been reported in LN nanophotonic waveguides leveraging the remarkable thermal-optic birefringence of LN [6]. In particular, a universal concept of a semi-nonlinear nanophotonic waveguide has also been demonstrated. By breaking the spatial symmetry of the nonlinear waveguide, intermodal PM between fundamental TE and second-order TE modes is realized [27]. Nevertheless, intermodal PM is intrinsically subject to poor spatial mode overlap, which inevitably degrades its conversion efficiency.

However, BPM can achieve exact phase matching, which makes use of the birefringence displayed by nonlinear media [28]. The refractive indices of fundamental wave (FW) and its SH can be equal in a proper light propagation direction with respect to the optical axis under a specific polarization configuration, with one being an ordinary wave and the other an extraordinary wave. However, the spatial walk-off effect greatly limits their interaction length in long bulk crystals, leading to a limited conversion efficiency. Additionally, BPM is a very restrictive condition to realize, and is rarely implemented in waveguides. To date, the method for BPM SHG at 1064 nm is mainly realized via temperature tuning [29–31] in which the BPM condition is closely met naturally. Perfect BPM in the telecommunication band is hardly involved in LNOI waveguides.

Here, we propose and demonstrate a novel design of angle-cut LN ridge waveguides for SHG on the LNOI platform, which can access type-I BPM without the need of periodic poling. A normalized conversion efficiency of 2.7%/W-cm^2 in the telecommunication C band is experimentally demonstrated. The approach effectively overcomes the spatial walk-off effect via the strong confinement of the waveguide, while possessing large mode overlap. It also gets rid of the complicated periodic poling of the LN waveguide. Furthermore, the strong thermo-optic effect in a type-I phase-matching scheme makes it possible to obtain a large wavelength tunability. The measured thermal tunability of the phase-matching wavelength is 1.06 nm/K, making it easy to cover the whole telecommunication C band by temperature control. The proposed angle-cut ridge waveguide structure can be applicable for other on-chip birefringent platforms as well, which is of great promise for efficient frequency conversion on integrated nonlinear photonics.

The designed angle-cut LN ridge waveguide based on the LNOI platform is schematically shown in Fig. 1(a). The on-top LN of the x-cut LNOI wafer has a thickness of 10 μm. The waveguide dimensions, as denoted in the inset of Fig. 1(a), are set as , $h_1 = 9\ \mu$m, $h_2 = 1\ \mu$m, $h_3 = 2\ \mu$m. The propagation direction of the ridge waveguide is tilted at an angle of θ with respect to the optical axis (c axis). The required angle-cut for a type-I process is given by $\sin^2\theta = \frac{(n_o^{\omega})^{-2}-(n_o^{2\omega})^{-2}}{(n_e^{2\omega})^{-2}-(n_o^{2\omega})^{-2}}$, where n_o^{ω}, $n_o^{2\omega}$, $n_e^{2\omega}$ are effective refractive indices of the FW and SH with subscripts denoting ordinary and extraordinary polarization, respectively [23]. Both the material and waveguide structure dispersion should be considered. The numerical calculated results at room temperature are plotted in Fig. 1(b). The phase-matching wavelength moves towards shorter wavelength rapidly as the angle increases, with 52° being an optimized cut angle for BPM in the telecommunication band in this case. Figure 1(c) shows the calculated effective indices of FW and SH at the optimized BPM angle to achieve the

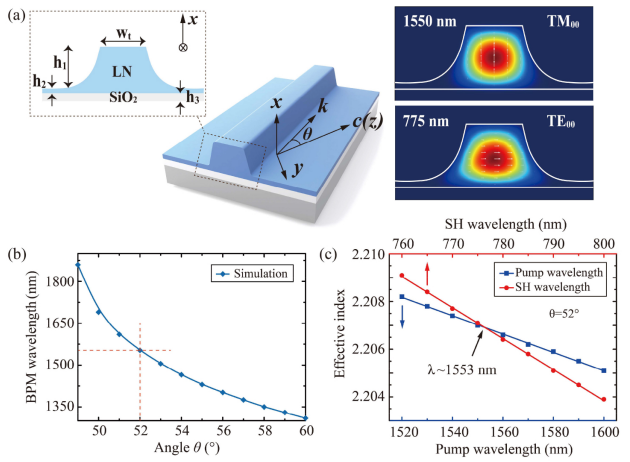

Fig. 1. (a) Schematic of the waveguide structure, and simulated mode profiles for FW and SH waves in the ridge waveguide. The arrows indicate the direction of polarization. (b) Numerically calculated BPM wavelength versus the propagation or cut angle at room temperature. (c) Effective indices of TM_{00} mode at FW (blue line) and TE_{00} mode at SH (red line) in the ridge waveguide.

exact BPM condition at around 1550 nm. The simulated mode profiles of TM_{00} at 1550 nm and TE_{00} at 775 nm are depicted in Fig. 1(a). The two modes have similar mode profile, inferring excellent mode overlapping. The calculated spatial mode overlap factor is ~0.98 between the FW and SH modes.

In our experiment, the sample is a 20-mm-long 52°-cut LN ridge waveguide on a LNOI wafer, which consists of 10-μm-thick LN bonded on top of a 2-μm-thick silica buffering layer above a silicon substrate. The ridge structure is formed between two 9-μm depth grooves using the optical grade dicing technique [32]. Figure 2(a) shows one end of the waveguide from a top-view microscope. The end facet of the waveguide is shown in Fig. 2(b), whose dimension is adopted in the numerical simulation, as shown in Fig. 1(a). The schematic of the experimental set-up is illustrated in Fig. 2(c). A continuous-wave (CW) tunable telecom-band laser (1520–1600 nm) amplified by an erbium-doped fiber amplifier (EDFA) is used as the pump. Light is controlled to excite the TM mode through a polarization controller (PC) and then launched into the waveguide, which is

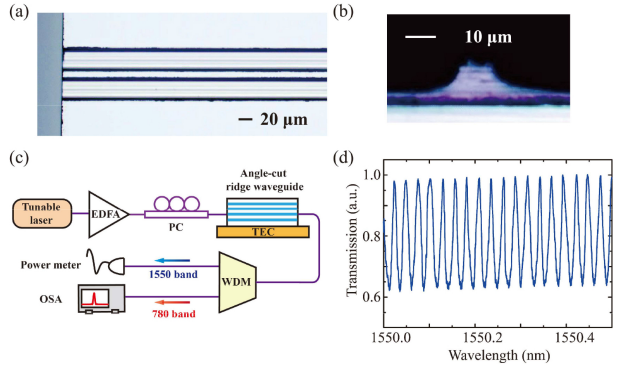

Fig. 2. (a) Microscopic image of the ridge waveguide from top view. (b) Cross section of the waveguide. (c) Schematic of the experimental setup. (d) Transmission spectrum of the waveguide in the telecommunication C band.

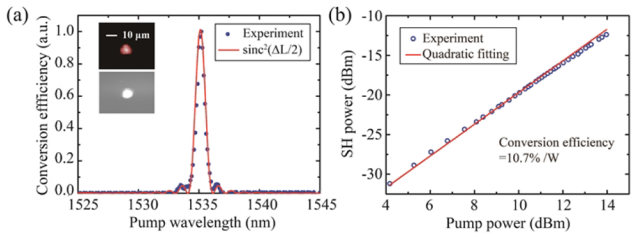

Fig. 3. (a) Measured SHG phase matching curve of the ridge waveguide. Inset shows the CCD images of the pump and SHG fundamental mode profiles at the output waveguide facet. (b) Measured SHG power versus the pump power with theoretical quadratic fitting.

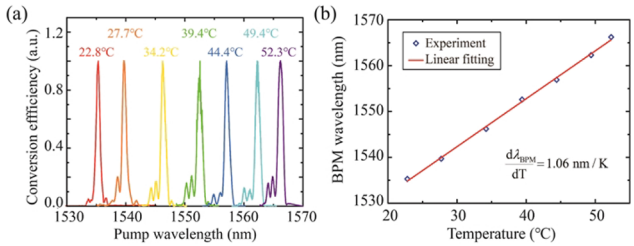

Fig. 4. (a) Measured SHG conversion efficiency spectra redshifts with increased temperatures. The spectra are normalized. (b) Temperature dependence of the BPM wavelength with the linear rate of 1.06 nm/K.

mounted on a thermoelectric cooler (TEC). Two single-mode fiber pigtails serve for the input and output coupling. At the output, the pump and the generated SH light are separated by a 780/1550 wavelength-division multiplexer (WDM). An optical spectrum analyzer (OSA) and a power meter are employed to detect and monitor the pump and SH light power.

We first investigate the linear optical properties of the fabricated angle-cut LN ridge waveguide. Figure 2(d) shows the measured transmission spectrum of the waveguide in the telecommunication C band for the TM mode. The total fiber-to-fiber loss is ~3.67 dB, including the waveguide propagation loss and facet coupling loss. The propagation loss is extracted to be approximately 0.42 dB/cm from the transmission curves when finely scanning the pump wavelength by using the Fabry– Pérot interference method [33,34], which is a small value for LN ridge waveguides.

Then we characterize the ridge waveguide's nonlinear performances in terms of SHG. Figure 3(a) presents the measured SHG efficiency spectrum as a function of the pump wavelength, indicating a phase-matched wavelength of 1535.1 nm and a bandwidth of approximately 0.8 nm at 22.8°C, well consistent with the theoretical prediction (sinc^2 function). Furthermore, the pump and generated SH with fundamental mode profiles are confirmed by direct imaging, as shown in the inset of Fig. 3(a), which suggests good spatial overlap between the interacting wave modes. This is critical for achieving a high conversion efficiency. The recorded SH power with respect to the pump power is plotted in Fig. 3(b), following a quadratic response in the low-conversion limit. An on-chip conversion efficiency of 10.7%/W in the 20-mm-long waveguide is experimentally obtained, corresponding to a normalized conversion efficiency of 2.7%/W-cm^2. The normalized conversion efficiency is defined as $P_{SH}/(P_{FH}^2 \cdot L^2)$, where P_{FH} and P_{SH} are the powers of FW and SH at the output, and L is the length of the waveguide.

The experimentally obtained normalized conversion efficiency in our case is smaller than the theoretical prediction due to several reasons. One reason lies in the imperfect cut angle along the waveguide. The simulation [Fig. 1(b)] infers that the phase-matching wavelength is highly sensitive with respect to the cut angle. The cut angle variation causes the phase-matching wavelength to vary along the waveguide, thus drastically affecting the overall SHG efficiency. In addition, the waveguide nonuniformity, especially the LN film thickness inhomogeneity, could also degrade the conversion efficiency. Meanwhile, the propagation loss and coupling loss of the generated SH light may be underestimated. Therefore, the measured conversion efficiency could be improved by further optimization of the cut angle with better uniformity. The optimized fabrication could be employed to increase the waveguide uniformity and smoothness by a chemical mechanical polishing technique.

Theoretically, the SHG conversion efficiency of the angle-cut BPM scheme is smaller than that of a type-0 configuration in periodically poled lithium niobate (PPLN) ridge waveguides under the same structure and dimension, for it uses d_{31} (~4.7 pm/V) of the nonlinear susceptibility, which is lower than the maximum component d_{33} (~27 pm/V). This may present a disadvantage in frequency conversion of continuous waves. However, for pulse lasers, whose peak power can easily reach over tens of watts, the overall conversion efficiency would become saturated and comparable regardless of BPM or QPM scheme. In contrast to the type-0 configuration, our waveguide in the BPM scheme is expected to exhibit a wide thermal tuning upon its temperature sensitivity, which is advantageous for tunable frequency convertors.

Finally, we study the thermal tuning capability of the ridge waveguide. Figure 4(a) plots the measured SHG conversion efficiency spectra at different temperatures. It clearly shows that the spectrum redshifts when the waveguide temperature increases, which represents a positive temperature dependence in the phase-matching wavelength. The strong side lobes may result from the slight nonuniformity of the waveguide along its total length [6,27]. By mapping the phase-matching wavelength as a function of temperature, a tuning slope of 1.06 nm/K is obtained, as shown in Fig. 4(b), which is larger than that obtained with type-0 SHG in LN by almost one order of magnitude [35]. The flexible tunability is highly useful for tunable coherent light generation applications.

In conclusion, we propose and demonstrate a novel design of angle-cut ridge waveguide for BPM SHG on the LNOI platform. The waveguide exhibits a normalized conversion efficiency of 2.7%/W-cm^2 in the experiment. Meanwhile, flexible tunability of the phase-matching wavelength is achieved with a tuning slope of 1.06 nm/K. The approach effectively avoids the spatial walk-off effect between ordinary and extraordinary waves due to tight confinement of the ridge waveguide. It drastically simplifies the waveguide fabrication and thus is beneficial to fabricate a high-performance waveguide with low propagation loss. In fact, it is not only restricted to the LN material, but can also be universally applied to other on-chip birefringent platforms, such as lithium tantalate (LT), potassium titanium phosphate (KTP), particularly other materials whose periodic poling is challenging. Therefore, we expect that the method may open up an avenue for nonlinear frequency conversion on integrated photonic that holds great promise for broad applications.

Funding. National Natural Science Foundation of China (12074252, 62005159, 62022058); National Key Research and Development Program of China (2018YFA0306301); Shanghai Municipal Science and Technology Major Project (2019SHZDZX01-ZX06); Shanghai Rising-Star Program (20QA1405400); Shandong Quancheng Scholarship (00242019024).

Disclosures. The authors declare no conflicts of interest.

Data availability. Data underlying the results presented in this paper are not publicly available at this time but may be obtained from the authors upon reasonable request.

REFERENCES

1. M. Jankowski, C. Langrock, B. Desiatov, A. Marandi, C. Wang, M. Zhang, C. R. Phillips, M. Lončar, and M. M. Fejer, Optica **7**, 40 (2020).
2. C. Wang, C. Langrock, A. Marandi, M. Jankowski, M. Zhang, B. Desiatov, M. M. Fejer, and M. Lončar, Optica **5**, 1438 (2018).
3. J. T. Lin, N. Yao, Z. Z. Hao, J. H. Zhang, W. B. Mao, M. Wang, W. Chu, R. B. Wu, Z. W. Fang, L. L. Qiao, W. Fang, F. Bo, and Y. Cheng, Phys. Rev. Lett. **122**, 173903 (2019).
4. J. Y. Chen, Z. H. Ma, Y. M. Sua, Z. Li, C. Tang, and Y. P. Huang, Optica **6**, 1244 (2019).
5. J. Y. Chen, C. Tang, Z. H. Ma, Z. Li, Y. M. Sua, and Y. P. Huang, Opt. Lett. **45**, 3789 (2020).
6. R. Luo, Y. He, H. Liang, M. Li, and Q. Lin, Optica **5**, 1006 (2018).
7. J. Zhao, C. Ma, M. Rüsing, and S. Mookherjea, Phys. Rev. Lett. **124**, 163603 (2020).
8. L. Caspani, C. Xiong, and B. J. Eggleton, Light: Sci. Appl. **6**, e17100 (2017).
9. J. Lu, M. Li, C. L. Zou, A. A. Sayem, and H. X. Tang, Optica **7**, 1654 (2020).
10. J. Wang, F. Sciarrino, A. Laing, and M. G. Thompson, Nat. Photonics **14**, 273 (2020).
11. J. T. Lin, F. Bo, Y. Cheng, and J. J. Xu, Photonics Res. **8**, 1910 (2020).
12. D. Zhu, L. Shao, M. Yu, R. Cheng, B. Desiatov, C. Xin, Y. Hu, J. Holzgrafe, S. Ghosh, A. Shams-Ansari, E. Puma, N. Sinclair, C. Reimer, M. Zhang, and M. Lončar, Adv. Opt. Photonics **13**, 242 (2021).
13. Y. Zheng and X. Chen, Adv. Phys.: X **6**, 1889402 (2021).
14. A. Honardoost, K. Abdelsalam, and S. Fathpour, Lasers Photonics Rev. **14**, 2000088 (2020).
15. C. Wang, M. Zhang, X. Chen, M. Bertrand, A. Shams-Ansari, S. Chandrasekhar, P. Winzer, and M. Lončar, Nature **562**, 101 (2018).
16. M. Zhang, B. Buscaino, C. Wang, A. Shams-Ansari, C. Reimer, R. Zhu, J. M. Kahn, and M. Lončar, Nature **568**, 373 (2019).
17. C. Wang, M. Zhang, M. Yu, R. Zhu, H. Hu, and M. Lončar, Nat. Commun. **10**, 978 (2019).
18. J. M. Dudley, G. Genty, and S. Coen, Rev Mod Phys. **78**, 1135 (2006).
19. Y. M. Sua, J. Y. Chen, and Y. P. Huang, Opt. Lett. **43**, 2965 (2018).
20. A. A. Sayem, Y. Wang, J. Lu, X. Liu, A. W. Bruch, and H. X. Tang, "Efficient and tunable blue light generation using lithium niobate nonlinear photonics," arXiv:2107.01171v1 (2021).
21. L. G. Carpenter, S. A. Berry, A. C. Gray, J. C. Gates, P. G. R. Smith, and C. B. E. Gawith, Opt. Express **28**, 21382 (2020).
22. C. Y. Cho, J. Y. Lai, C. S. Hsu, Y. T. Huang, J. H. Jang, and M. H. Chou, Opt. Lett. **46**, 2852 (2021).
23. A. Rao, K. Abdelsalam, T. Sjaardema, A. Honardoost, G. F. Camacho-Gonzalez, and S. Fathpour, Opt. Express **27**, 25920 (2019).
24. J. Lu, J. B. Surya, X. Liu, A. W. Bruch, Z. Gong, Y. Xu, and H. X. Tang, Optica **6**, 1455 (2019).
25. J.-Y. Chen, Y. M. Sua, Z.-H. Ma, C. Tang, Z. Li, and Y.-P. Huang, OSA Continuum **2**, 2914 (2019).
26. L. Chang, Y. F. Li, N. Volet, L. R. Wang, J. Peters, and J. E. Bowers, Optica **3**, 531 (2016).
27. R. Luo, Y. He, H. Liang, M. Li, and Q. Lin, Laser Photon. Rev. **13**, 1800288 (2019).
28. R. W. Boyd, *Nonlinear Optics* (Elsevier, 2019).
29. T. Pliska, D. Fluck, P. Gunter, E. Gini, H. Melchior, L. Beckers, and C. Buchal, Appl. Phys. Lett. **72**, 2364 (1998).
30. J. Burghoff, C. Grebing, S. Nolte, and A. Tünnermann, Appl. Phys. Lett. **89**, 081108 (2006).
31. B. Zhang, L. Li, L. Wang, and F. Chen, Opt. Mater. **107**, 110075 (2020).
32. N. Courjal, F. Devaux, A. Gerthoffer, C. Guyot, F. Henrot, A. Ndao, and M.-P. Bernal, Opt. Express **23**, 13983 (2015).
33. C. Wang, X. Xiong, N. Andrade, V. Venkataraman, X.-F. Ren, G.-C. Guo, and M. Lončar, Opt. Express **25**, 6963 (2017).
34. R. Regener and W. Sohler, Appl. Phys. B **36**, 143 (1985).
35. M. M. Fejer, G. Magel, D. H. Jundt, and R. L. Byer, IEEE J. Quantum Electron. **28**, 2631 (1992).